Prepared for submission to JCAP

arXiv:1406.6875v1 [astro-ph.GA] 26 Jun 2014

Is Sextans dwarf galaxy in a scalar field dark matter halo?

V. Lora[a] **and Juan Magaña**[b]

[a]Astronomisches Rechen-Institut, Zentrum für Astronomie der Universität Heidelberg, Mönchhofstr. 12-14, 69120 Heidelberg, Germany

[b]Instituto de Física y Astronomía, Facultad de Ciencias, Universidad de Valparaíso, Av. Gran Bretaña 1111, Valparaíso, Chile

E-mail: vlora@ari.uni-heidelberg.de, juan.magana@uv.cl

Abstract. The Bose-Einstein condensate/scalar field dark matter model, considers that the dark matter is composed by spinless-ultra-light particles which can be described by a scalar field. This model is an alternative model to the Λ-cold dark matter paradigm, and therefore should be studied at galactic and cosmological scales. Dwarf spheroidal galaxies have been very useful when studying any dark matter theory, because the dark matter dominates their dynamics. In this paper we study the Sextans dwarf spheroidal galaxy, embedded in a scalar field dark matter halo. We explore how the dissolution time-scale of the stellar substructures in Sextans, constrain the mass, and the self-interacting parameter of the scalar field dark matter boson. We find that for masses in the range $(0.12 < m_\phi < 8) \times 10^{-22}$ eV, scalar field dark halos without self-interaction would have cores large enough to explain the longevity of the stellar substructures in Sextans, and small enough mass to be compatible with dynamical limits. If the self-interacting parameter is distinct to zero, then the mass of the boson could be as high as $m_\phi \approx 2 \times 10^{-21}$ eV, but it would correspond to an unrealistic low mass fot the Sextans dark matter halo . Therefore, the Sextans dwarf galaxy could be embedded in a scalar field/BEC dark matter halo with a preferred self-interacting parameter equal to zero.

Keywords: dark matter theory, dark matter simulations, dwarf galaxies

Contents

1 Introduction **1**
1.1 The BEC/SFDM halos 2

2 Sextans and its stellar substructures **5**

3 The modelling of Sextans **5**
3.1 Sextans' Dark Matter component 5
3.2 Sextans' stellar substructures 6
3.3 The N-body code 7

4 Results **7**
4.1 The $\Lambda = 0$ case 7
4.2 The small $\Lambda \neq 0$ case 10

5 Conclusions **11**

1 Introduction

The nature of dark matter (DM) is a puzzle in modern Cosmology. The standard interpretation supposes that DM is made up of weakly interacting massive particles which are non-relativistic at the epoch of decoupling (i.e., cold DM; hereafter CDM).

Despite the predictions of the CDM are in agreement with several cosmological observations, it has fundamental inconsistencies which remain to be solved. A popular example is the well-known overpopulation of dark substructure [1]. Nevertheless, there are many other less-known questions that the CDM model cannot explain. The expected number of galaxies in the local void [2], is one example. The observational data at galactic scales seem to disagree with CDM predictions, when comparing the density profiles of dark halos predicted in simulations with those derived from observations of dwarf spheroidal (dSph) galaxies and Low Surface Brightness galaxies (LSB's). N-body simulations predict a universal cuspy density profile, while observations indicate that a cored halo is preferred in an important fraction of low-mass galaxies [3–5]. This discrepancy is known as the cusp/core problem.

The failures of the CDM model have motivated the study of several DM alternatives. Lately, a hypothesis that has gained interest is to consider that DM is made up bosons described by a real (or complex) scalar field Φ. Such paradigm is called the scalar field DM (SFDM) model [6–13].

In the SFDM model, the scalar field Φ is minimally coupled to gravity and interacts only gravitationally with the baryonic matter. In the early Universe, the scalar field is in a thermal bath of temperature T. When a critical temperature T_c is reached, the scalar field has a symmetry breaking and possibly a phase transition. This phase transition can be interpreted as the condensation of the scalar field [14–17](BEC/SFDM model). After this stage, the scalar field is driven towards a minimum of the potential. Once the scalar field reaches the minimum ($T \ll T_c$), and if the mass of the boson associated to the scalar field Φ is greater than the expansion rate of the Universe ($m_\phi \gg H$), then the scalar field has a fast oscillation phase [18]. At this regime, if the boson mass is in the range $m_\phi \sim 10^{-23} - 10^{-21}$

eV, the SFDM behaves as CDM and their linear perturbations evolve as those in the standard CDM model [19–22]. Moreover, due to the fact that the effective Jeans length for a scalar field depends on the boson mass as $\lambda_J \sim m_\phi^{-1}$, the mass power spectrum has a natural cut-off and the overpopulation of substructures is avoided in a natural way.

The dynamics of the BEC/SFDM model at cosmological and galactic scales, have been studied both, theoretically and numerically [23–28] to put constraints on the free parameters of the model: mainly the SFDM boson mass. For example, [29] found that the SFDM model is consistent with the anisotropies of the cosmic microwave background radiation (CMB), if the mass of the boson is $m_\phi \sim 10^{-22}$ eV. [30], study the vortex formation in BEC/SFDM halos, including the angular momentum, obtaining a window for the mass of the boson of $10^{-21} - 10^{-23}$ eV, for dwarf-galaxy-sized halos.

Recently, Li et al. [31] put constraints on a complex SFDM model, using the effective number of neutrino species during the Big Bang nucleosynthesis, obtaining $m_\phi \geq 2.4 \times 10^{-21}\mathrm{eV}/c^2$ and $9.5 \times 10^{-19}\mathrm{eV}^{-1}\mathrm{cm}^3 \leq \lambda/(m_\phi c^2)^2 \leq 4 \times 10^{-17}\mathrm{eV}^{-1}\mathrm{cm}^3$.

[32] use the internal stellar structures of dwarf spheroidal (dSph) galaxies to establish a preferred range for the mass m_ϕ of the bosonic particle. They performed N-body simulations of the Ursa Minor (UMi) dSph and explored how the dissolution time-scale of the cold stellar clump in UMi depends on m_ϕ. They found that for a mass in the range of $(0.3 < m_\phi < 1) \times 10^{-22}$ eV, the BEC/SFDM model would have large enough cores to explain the longevity of the cold stellar clump in UMi, and the wide distribution of globular clusters in the Fornax dSph.

On the other hand, [33] fit the high-resolution rotation curves of a sample of 13 low-surface-brightness galaxies, obtaining a better fit with the SFDM/BEC model over the NFW [34] profile. The BEC/SFDM has proved to be a promising DM alternative. Nevertheless, further tests are needed in galactic systems dominated by DM, such as the dSph galaxies of the Local Group (LG).

There has been recent evidence of stellar substructure in other dSph galaxy: Sextans. [35] reported the existence of a dissolving cluster at the centre of Sextans. Later on, [36] detected a region near Sextans core radius that appeared kinematically colder than the overall stellar population of Sextans. Recently, [37] reported a nine-star group of very metal-poor stars which they suggest could be in fact the same substructure previously found by [35].

In this work we will perform N-body simulations of the Sextans dSph galaxy, embedded in a rigid SFDM halo. The survival of the stellar clump in Sextans will give us dynamic constraints on the mass m_ϕ and on the self-interacting parameter λ.

The article is organised as follows. In §1.1 we describe the SFDM model and briefly review the Schrödinger-Poisson system. We present the characteristics of Sextans and its stellar clump in §2. In §3, we discuss the DM for Sextans, the set-up for the N-body models, and describe the code used. In §4, we describe our results. Finally, in section §5 we discuss the results and give our conclusions.

1.1 The BEC/SFDM halos

The BEC/SFDM forms relativistic and Newtonian configurations in equilibrium, which can be interpreted as DM halos. In the relativistic regime, these gravitational structures, described by the Einstein-Klein-Gordon (EKG) equations, are known as boson stars (for complex scalar fields) and oscillatons (for real scalar fields). Several numerical studies [38, 39]

have shown that both structures have a critical mass $M_{crit} \sim 0.6 \left(\frac{m_P}{m_\phi}\right) \sim 10^{12}$ M$_\odot$, a typical-galaxy size, for an ultra-light boson with mass m_ϕ, and $m_P = \sqrt{\hbar c/G}$ the Planck mass.

In this work, we study the dynamics of the Sextans dSph, which is well described by a Newtonian gravitational configuration. We model the BEC/SFDM halos, by performing the weak field and low velocity limit of the EKG equations, for a complex scalar field Φ, endowed with a self-interacting potential $V(\Phi) = m^2\Phi^2/2 + \lambda\Phi^4/4$. This leads to the Schrödinger-Poisson system:

$$i\hbar\frac{\partial\psi}{\partial t} = -\frac{\hbar^2}{2m_\phi}\nabla^2\psi + Um_\phi\psi + \frac{\lambda}{2m_\phi}|\psi|^2\psi \ , \tag{1.1}$$

$$\nabla^2 U = 4\pi G m_\phi^2 \psi\psi^* \ . \tag{1.2}$$

In the latter equations, m_ϕ is the mass of the boson associated to Φ. U is the gravitational potential produced by the DM density source ($\rho = m_\phi^2|\psi|^2$), λ is the self-interacting coupling constant, and the field ψ is related to the relativistic field Φ through $\Phi = e^{-im_\phi c^2 t/\hbar}\psi$ [40–42].

To construct spherical BEC/SFDM halos in equilibrium, we assume $\psi(r,t) = e^{-i\gamma t/\hbar}\phi(r)$, reducing the Schrödinger-Poisson system to an eigenvalue problem for $\phi(r)$.

Using the dimensionless variables

$$\begin{aligned}
\hat{\phi} &= \sqrt{4\pi G\hbar}\frac{\phi}{c^2} \\
\hat{r} &= \frac{m_\phi c r}{\hbar} \\
\hat{t} &\equiv \frac{m_\phi c^2 t}{\hbar} \\
\hat{U} &\equiv \frac{U}{c^2} \\
\Lambda &= \frac{m_P^2 c\lambda}{8\pi m_\phi \hbar^3} \\
\hat{\gamma} &= m_\phi c^2 \gamma \ ,
\end{aligned} \tag{1.3}$$

then, the Schrödinger-Poisson system now reads as,

$$\frac{d^2}{d\hat{r}^2}(\hat{r}\hat{\phi}) = 2\hat{r}(\hat{U} - \hat{\gamma}) + 2\hat{r}\Lambda\hat{\phi}^3 \ , \tag{1.4}$$

$$\frac{d^2}{d\hat{r}^2}(\hat{r}\hat{U}) = \hat{r}\hat{\phi}^2 \ . \tag{1.5}$$

Following [43] we construct SFDM halos by obtaining ground state solutions of the system (1.4-1.5). The mass of this BEC/SFDM halo can be estimated as

$$M = \int_0^\infty \hat{\phi}^2\hat{r}^2 d\hat{r}. \tag{1.6}$$

In addition, we define the radius of this configuration as r_{95}, the radius containing 95% of the mass. Note that both properties, the mass and the radius, of the scalar halo depend on the

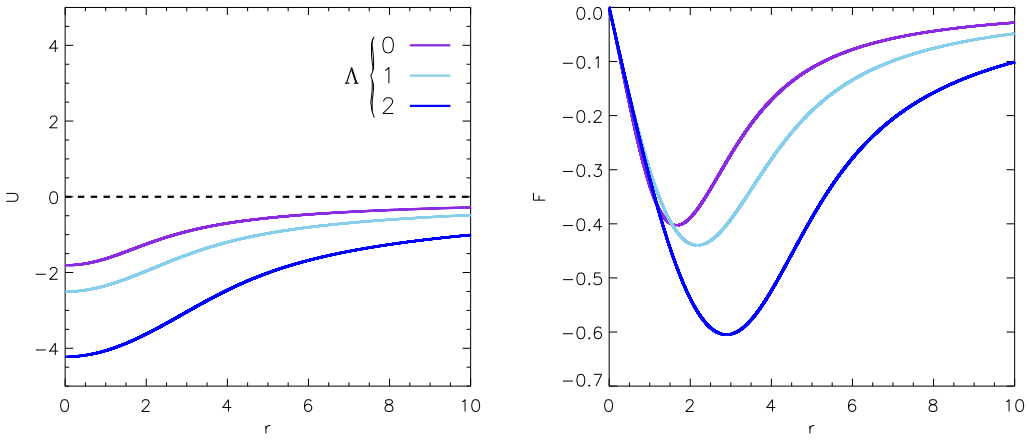

Figure 1. Potential and force associated to the SFDM, for ground states, for the values of the self interacting parameter $\Lambda = 0, 1$ and 2 in dimensionless units.

boson mass, and the self-interacting term. Thus, to model the Sextans halo with several m_ϕ and Λ values, we use the invariance of the Schrödinger-Poisson system under the following scaling

$$\begin{aligned} \hat{\phi} &\to \epsilon^2 \hat{\phi} \\ \hat{U} &\to \epsilon^2 \hat{U} \\ \hat{\gamma} &\to \epsilon^2 \hat{\gamma} \\ \Lambda &\to \epsilon^2 \Lambda \\ \hat{r} &\to \epsilon^{-1} \hat{r} \\ \hat{M} &\to \epsilon \hat{M} \ . \end{aligned} \tag{1.7}$$

It is worth mentioning that the excited state solutions of the Schrödinger-Poisson system are unstable. Thus, we only model the Sextans halo with ground state scalar configurations. In Figure 1, we show the potential and the force (in dimensionless units) associated to the SFDM, for ground states for three different values of the self interacting parameter Λ.

Additionally, the Schrödinger-Poisson equations could be interpreted as the mean-field approximation at zero temperature of the Gross-Pitaevskii-Poisson (GPP) system, governing the dynamics of a Newtonian BEC. In the BEC interpretation, U is the trapping potential of the BEC, and the coupling constant λ, is related to s-wave scattering length a of the bosons. The regime where the self-interacting term strongly dominates the GP equation, is called the Thomas-Fermi limit (TFL). For a static BEC in the TFL, the GP reduces to a Lane-Emden (LE) equation, which has an analytical solution, when the BEC has a polytropic equation of state (EoS) with index $n = 1$. In this case, the BEC density profile is $\rho_{BEC}(r) \propto \frac{sin(r/r_{max})}{r/r_{max}}$, where r_{max}, the maximum size of the gravitational structures, depend on m and λ. Although these configurations are widely used, Guzmán et al. [44] claim that they are unstable and dissipate in a short time (see also the discussion by [45]). Nevertheless, [46] found that the stability of BEC halos in the TFL depend on the mass and the scattering length of the particle. In this work we do not consider the TFL solutions.

2 Sextans and its stellar substructures

The Sextans dSph galaxy satellite of the Milky Way is located at a Galactocentric distance of $R_{GC} = 86$ kpc [47] and it has a luminosity of $L_V = (4.37 \pm 1.69) \times 10^5$ $L_\odot$ [48]. It has a core radius of $R_{core} \simeq 0.4$ kpc and a tidal radius of $R_{tidal} \simeq 4$ kpc [49]. It has a stellar mass of $\sim 8.9 \pm 4.1 \times 10^5$ $M_\odot$ [50]. The values of the mass and luminosity of Sextans give a typical stellar mass-to-light ratio of $\Upsilon_\star \approx 2$.

Based on the velocity dispersion profile, [51] obtain a $M/L \sim 130$ $(M/L)_\odot$. On the other hand, [52] estimate a $M/L \sim 260$ $(M/L)_\odot$, and [48] obtain a M/L value of ~ 96 $(M/L)_\odot$. The latter studies based on Sextans' internal dynamics, suggest that the Sextans dwarf is a highly DM dominated dSph.

Sextans is also very interesting because it contains (at least) two stellar substructures. [35] found that the velocity dispersion at the centre of Sextans was close to zero, and that such a low value of the dispersion was in agreement with significant radial gradients in the stellar populations (change in the ratio of red horizontal branch stars to blue horizontal branch stars). They suggested that this is caused by the sinking and gradual dissolution of a star cluster at the centre of Sextans.

On the other hand, [36] presented radial velocities of 294 possible Sextans members. Their data did not confirm [35]'s report of a kinematically distinct stellar population at the centre of Sextans with their more complete sample. Instead, they detect a region near Sextans core radius (~ 0.4 kpc) kinematically colder than the overall Sextans sample with 95% confidence.

Lately, [37] reported nine old stars that share very similar spatial location, kinematics, and metallicities, being the substructure's average metallicity $[Fe/H] = -2.6$ dex. This stellar substructure is consistent with being a remnant of an old stellar cluster, with a luminosity of 2.2×10^4 $L_\odot$.

The present spatial extent of the substructures is very uncertain. The contours of statistical significance for regions of cold kinematics [36] show that their stellar substructure is centred on a location 15 arcmin north of the Sextans centre and has a radial size of 4 arcmin (~ 100 pc). On the other hand, the nine innermost metal-poor stars that constitute [37] substructure, are found at $R < 0\,^\circ.22$, i.e., at ≈ 330 pc.

Since we do not know the orbital parameters of the substructures, we explored different orbits for the clumps around the Sextans centre. We only know lower limits for the semi-major axes of the substructures (~ 400 pc for [36] substructure, and ~ 200 pc for [37] substructure). Since the substructures are not necessarily on circular orbits, we also consider the case of eccentric orbits.

3 The modelling of Sextans

3.1 Sextans' Dark Matter component

[37] computed the DM mass models for Sextans, based on their best-fitting of their observed line-of-sight velocity dispersion profile. They found that for a NFW [34] DM model, the best fitting model corresponds to a concentration $c = 10$ and a virial mass $M_V = 2.6 \times 10^9$ $M_\odot$. They also fit their data to a cored DM profile. For the best fitting, they obtained a cored radius $r_c = 3$ kpc, and a mass within the last measured point (~ 2.3 kpc assuming a distance to Sextans of 86 kpc; Mateo 1998) of $M(< R_{last}) = 4 \times 10^8$ $M_\odot$.

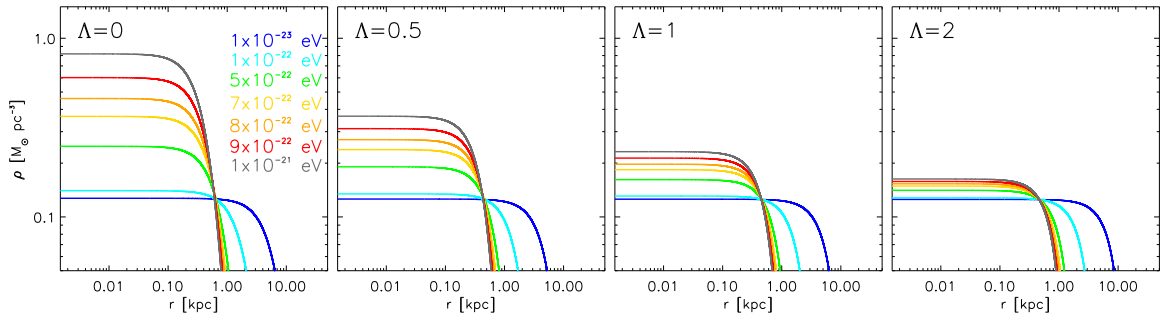

Figure 2. We show the density profile of the SFDM halo for Sextans dwarf galaxy, for different values of the mass of the boson m_ϕ, and for the self-interacting parameters $\Lambda = 0$, 0.5, 1 and 2.

[52, 53] compute the Sextans' DM mass within 0.6 kpc, $M(< 0.6) = 0.9 \pm 0.4 \times 10^7$ $M_\odot$, for a CDM model. [37] obtained a mass $M(< 0.6) = 2 \pm 0.6 \times 10^7$ $M_\odot$, for their best-fitting NFW model. They also find an enclosed mass of $M(< 0.6) = 0.9 \pm 0.2 \times 10^7$ $M_\odot$ for their best-fitting cored DM profile, very similar to [52]'s mass estimate. Therefore, to construct the Sextans' SFDM halo, we impose that the halo mass within 0.6 is $M(< 0.6) = 9 \times 10^6$ $M_\odot$.

In Figure 2, we show the Sextans' SFDM density profile (for $\Lambda = 0$, 0.5, 1 and 2) for different mass of the boson m_ϕ. From this Figure, we can see that for a self interacting parameter $\Lambda = 0$, the central density is $\rho_0 \approx 0.8$ $M_\odot$ pc^{-3}, for $m_\phi = 10^{-23}$ eV. For larger values of the self interacting parameter, for example $\Lambda = 2$, the central density for the same mass of the boson $m_\phi = 10^{-23}$ eV, is $\rho_0 \approx 0.16$ $M_\odot$ pc^{-3}. The value of the central density drops when Λ increases. We define the SFDM core radius, as the radius at which the central density has dropped a factor 2 (see Table 1). We can see from Figure 2, that for a fixed mass of the boson m_ϕ (say 10^{-21} eV), the core radius for $\Lambda = 0$ is $r_{core} = 0.34$ kpc. Whereas, for the same m_ϕ and $\Lambda = 2$, the core radius is $r_{core} = 0.71$. The value of the core radius increases when Λ increases, for a fixed value of m_ϕ.

Recently, [54] analysed the Aquarius simulations to characterize the shape of the DM halos with maximum circular velocities between 8 and 200 km/s. They found that DM sub-halos, comparable to those hosting classical dSph galaxies in the LG, are mildly triaxial with $(b/a) \sim 0.75$ and $(c/a) \sim 0.6$ at $r \sim 1$ kpc. Therefore, as a first approximation, it is a reasonable assumption to adopt an spherical BEC/SFDM DM halo for the Sextans dSph.

3.2 Sextans' stellar substructures

For the initial mass density profile of the stellar clump, we used a Plummer [55] mass density profile given by the following equation:

$$\rho_c(r) = \rho_0 \left(1 + \left(\frac{r}{r_p}\right)^2\right)^{-5/2} . \tag{3.1}$$

The present spatial extent of the substructures is very uncertain. The contours of statistical significance for regions of cold kinematics in [36] show, that their substructure is located at ~ 375 arcmin north of the Sextans centre, and has a radial size of ~ 100 pc.

On the other hand, the nine innermost metal-poor stars that conform the stellar clump [37], are found at $R < 0°.22$ (~ 330 pc, if we assume a distance to Sextans of 86 kpc; Mateo 1998). In Battaglia et al.'s (2011) data, there are no metal-poor stars within $R < 0°.1$, which suggests that the stellar substructure extends in projected galactocentric radius from

0°.1 to 0°.22 (equivalent to 150 − 330 pc). Indicating that, in projection, its centre is at ∼ 240 pc from the centre of Sextans, with a radius (at most) of ∼ 90 pc.

We assume that the V-band mass-to-light ratio M/L_V of the clump is the same as it is for the underlying stellar component ($\Upsilon_\star = 2$). A crude estimate of the stellar substructures' total luminosity is $L_c = 2.2 \times 10^4$ L$_\odot$ [37], then, a mass of the clump $M_c \simeq 4.4 \times 10^4 M_\odot$ is obtained.

We run sets of simulations varying the plummer radius of the clump (5, 35 and 80 pc). We drop the stellar clumps in a circular orbit with a galactocentric distance of 0.4 kpc, mimicking the stellar substructure found by [36]. Then, we drop the stellar clumps at a galactocentric distance of 0.2 kpc in a circular orbit, representing the stellar substructure found by [37]. Finally, we explore the possibility that a stellar substructure could be in an eccentric orbit with an apocenter distance from the centre of Sextans of 0.4 kpc, and a pericenter distance of 0.1 kpc (which corresponds to an eccentricity of $e = 0.6$).

3.3 The N-body code

The crossing time is defined as

$$t_{cross} = 2\pi \frac{R_c^{3/2}}{\sqrt{GM_c}} \ , \tag{3.2}$$

then the relaxation time can be defined as a function of the crossing time,

$$t_{relax} \simeq \frac{0.1N}{lnN} \times t_{cross} \ . \tag{3.3}$$

The relaxation times for both clumps radii are $\gtrsim t_H$ therefore the two-body relaxation processes can be neglected and the system can be represented as collisionless [56]. We simulated the evolution of the Sextans' stellar clump embedded in a rigid SFDM halo potential, using the N-body code SUPERBOX [57, 58]. SUPERBOX is a highly efficient particle-mesh, collisionless-dynamics code with high resolution sub-grids. In our case, SUPERBOX uses three nested grids centred in the centre of density of the Sextans' stellar clump. We used 128^3 cubic cells for each of the grids. The inner grid is meant to resolve the inner region of Sextans' clump, and the outer grid (with radii of 10 kpc) resolves the stars that are stripped away from Sextans' clump. The spatial resolution is determined by the number of grid cells per dimension (N_c) and the grid radius ($r_{\rm grid}$). Then the side length of one grid cell is defined as $l = \frac{2r_{\rm grid}}{N_c - 4}$. For $N_c = 128$, the resolution is 0.5 pc. SUPERBOX integrates the equations of motion with a leap-frog algorithm, and a constant time step dt. We selected a time step of $dt = 0.1$ Myr in our simulations in order to guarantee that the energy is conserved better than 1%.

4 Results

4.1 The $\Lambda = 0$ case

We ran N-body simulations from $t = 0$ to $t = 10$ Gyr, of the stellar clump in the Sextans dwarf (for three different plummer radius; 5, 35 and 80) embedded in a SFDM halo, with a self-interacting parameter $\Lambda = 0$, varying the mass of the boson m_ϕ. As we mentioned before, we selected three different types of orbits; A circular orbit at a galactocentric distance of 0.4 kpc, a circular orbit with a galactocentric distance of 0.2 kpc, and an eccentric orbit with $e = 0.6$. All the stellar-clump-models, orbit in the (x, y)-plane. In order to quantify the destruction time Π of the stellar clump in Sextans, we build a map of the surface mass

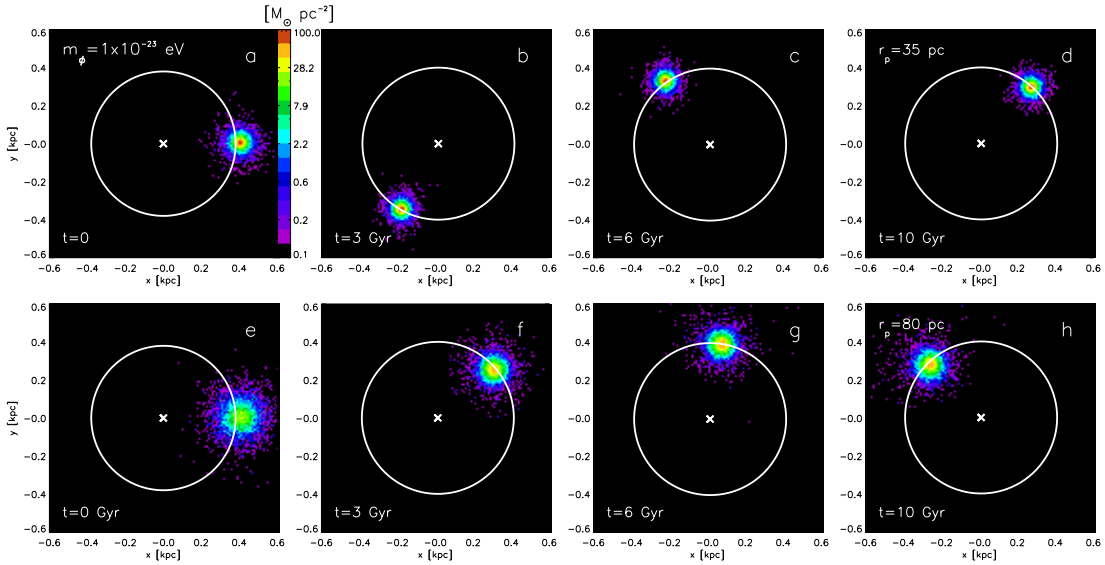

Figure 3. Time evolution (t = 0, 3, 6 and 10 Gyr) of the stellar clump's surface mass density in the Sextans dSph. In the top panels we show the evolution of the clump with r_c = 35 pc, and in the bottom panels we show the time evolution of model with r_c = 80 pc. The white circle shows the initial orbit with 0.4 kpc radius. The white cross marks the centre of Sextans. We set the clump on a circular orbit in the (x, y)-plane at a distance of $r = 0.4$ kpc from Sextans' centre. The mass of the boson is $m_\phi = 10^{-23}$ eV and the self interacting parameter is $\Lambda = 0$, which corresponds to a total mass of the galaxy $M = 6.28 \times 10^9 M_\odot$ (see Table 1).

density (in units of $M_\odot$ pc^{-2}) of the stellar clump in the (x, y)-plane, for every time t in the simulation. When the surface mass density falls below the value ~ 1.5 $M_\odot$ pc^{-2}, which is the typical surface mass density of the underlying stellar component in Sextans, we define that the stellar clump is destroyed (i.e., at this value, the particles in the clump would not be recognizable form the particles of the main stellar component in Sextans). In the top panels of Figure 3, we show the time evolution of the surface mass density of the clump at t = 0, 3, 6 and 10 Gyr, for the model with $m_\phi = 10^{-23}$ eV in a circular orbit at a galactocentric distance of 0.4 kpc. The stellar clump has an initial plummer radius, r_p = 35 pc. Such a location of the clump, resembles the stellar substructure found by [36]. The white line shows the initial orbit of the stellar clump, and the white cross shows the centre of Sextans.

We see that the clump remains intact for $\sim$ 10 Gyr. In the lower panels of Figure 3, we show the time evolution of the stellar clump with a radius r_p = 80 pc. Also in this extended-radius case, the clump remains unchanged for $\sim$ 10 Gyr. The survival of both stellar clumps is a consequence that the SFDM halo has a very large core ($\sim$ 5.4 kpc; see Table 1), that guarantees the survival of the clump [4, 32]. In Table 1, we give the mass of the SF boson, the properties of the SFDM halos, the destruction time (Π) for each clump radius case, and the orbit of the stellar clump.

There is a positive correlation between the size of the SFDM core radius (r_{core}), and the maximum of the circular velocity ($V_{\rm max}$). Large values of the core are favoured to explain the persistence of the stellar clump, but they require very large values of $V_{\rm max}$ and thus, the total DM halo mass. For example, for a SF boson mass of $m_\phi = 10^{-23}$ eV the total dynamical mass is $M \approx 6.3 \times 10^9$ $M_\odot$, and therefore, $V_{\rm max} \simeq 52$ km s^{-1}. But a value of $V_{\rm max} \simeq 8 - 12$ km s^{-1} is computed for Sextans dwarf [59–61], which indicates that the latter

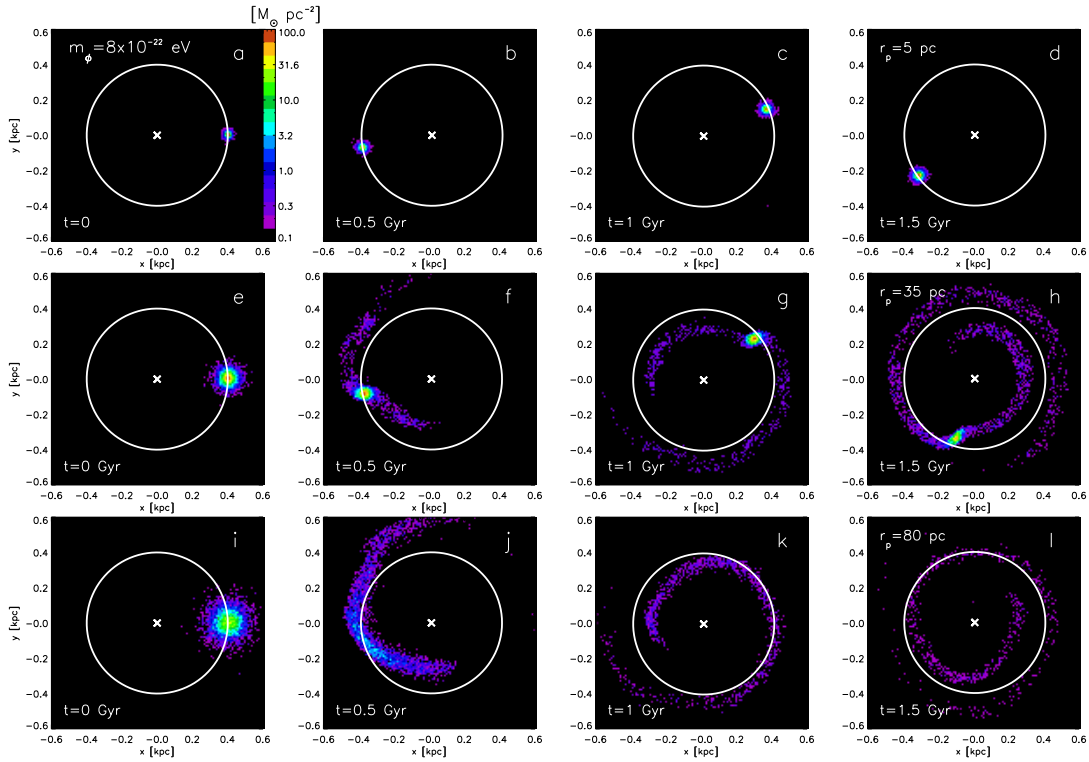

Figure 4. Time evolution ($t = 0$, 0.5, 1 and 1.5 Gyr) of the stellar clump's surface mass density in the Sextans dSph. In the top panels (*a*-*d*) we show the evolution of the compact $r_c = 5$ pc clump. In the middle panels (*e*-*h*) we show the time evolution of model with $r_c = 35$ pc. In the bottom panels (*i*-*l*) we show the time evolution for the extended model with a radius $r_c = 80$ pc. The white circle shows the clump orbit, and the white cross marks the centre of Sextans. We set the clump in a circular orbit, in the (x, y)-plane, at a galctocentric distance of 0.4 kpc. In this case, the mass of the boson is $m_\phi = 8 \times 10^{-22}$ eV and the self interacting parameter is $\Lambda = 0$, which corresponds to a total mass of the galaxy $M \sim 1.2 \times 10^7 M_\odot$ (see Table 1).

DM halo is too massive.

Moreover, [37] suggest that Sextans' DM halo virial mass, derived from the assumption of a NFW model, is $\sim 2.6 \times 10^9 M_\odot$. This is a factor ~ 2 smaller, than the mass of the halo that we find for a $m_\phi = 10^{-23}$ eV. [59] point out, that only 5% of the sub-halos in a Milky Way-sized halo have a total mass $M > 5 \times 10^9 M_\odot$. Therefore, 5×10^9 M$_\odot$ is a natural first upper limit to the mass of Sextans DM halo [32]. Adopting the latter maximum value for the mass, we obtain a lower limit to the mass of the boson of $m_\phi \gtrsim 1.2 \times 10^{-23}$ eV.

Both, the shape of the underlying gravitational potential, and the longevity of the clump, depend on the mass of the SF boson m_ϕ. Since both, the size of the DM core, and the total mass increase when m_ϕ decreases, the next step is to consider the evolution of the clump in models with larger values of m_ϕ.

We increase the mass of the boson one order of magnitude to $m_\phi = 10^{-22}$ eV. The stellar clump (for the three different radius; 5, 35 and 80 pc) also remains undisturbed for ~ 10 Gyr. The corresponding core radius and mass are, 1.7 kpc and $\sim 2 \times 10^8$ M$_\odot$, respectively (see Table 1). With the latter data, we compute a $V_{\rm max} \simeq 17$ km s^{-1}, still large for Sextans, but close enough to set a better lower limit to the mass of the SF boson.

Next, we rise the value of the mass of the SF boson to $m_\phi = 5 \times 10^{-22}$ eV. We observe

that the clump with $r_p = 35$ pc looses some particles but remains without much damage for a Hubble time. On the other hand, for the extended $r_p = 80$ case, the clump suffers a drastic damage, and appears almost destroyed by ~ 10 Gyr. Then, we rise the value of m_ϕ to 8×10^{-22} eV, the clump (for radius $r_p = 35$ and 80 pc) is destroyed within 2 Gyr, due to strong tidal effects (see Figure 4). But a compact stellar clump with $r_p = 5$ pc survives for 10 Gyr. The $m_\phi = 8 \times 10^{-22}$ eV case has a value for the core radius of ~ 0.5 kpc and $V_{\rm max} \simeq 8$ km s^{-1}, which is in agreement with the value given by [59].

It has to be noted that the stellar clump with $r_p = 5$ and 35 pc remains without being destroyed for the adopted mass range $m_\phi = 10^{-23} - 10^{-21}$ eV, when the clump is orbiting at a galactocentric distance of 0.2 kpc (similar to Battaglia et al.'s 2011 substructure case). The fact that the clump is located well inside the SFDM core radius, guarantees its longevity. Even the extended $r_p = 80$ pc case survives for 3 Gyr, when orbiting so close to the centre of the SFDM potential of Sextans.

For the eccentric orbit case, the clumps with $r_p = 35$ and 80 pc get destroyed when $m_\phi = 8 \times 10^{-22} - 10^{-21}$ eV. The $r_p = 5$ pc clump gets destroyed when we raise the mass of the boson to $m_\phi = 9 \times 10^{-22} - 10^{-21}$ eV (see Table 1).

The survival of the stellar substructures in Sextans set an upper limit to the mass of the boson of $m_\phi < 8 - 9 \times 10^{-22}$ eV. The destruction times, for each of m_ϕ cases are given in Table 1. We conclude that the mass of the boson in the $\Lambda = 0$ case lays in the range $10^{-21} < m_\phi < 8 \times 10^{-22}$ eV.

4.2 The small $\Lambda \neq 0$ case

In the subsection 4.1, we assumed that the boson self-interaction is negligible ($\Lambda = 0$). In order to see how m_ϕ depends on self-interaction, we explore models with the third term of Equation 1.1 being distinct from zero ($\Lambda \neq 0$). We consider only small values of Λ (in dimensionless units 0.5, 1 and 2). The parameters of the models are summarized in Table 1.

For a $\Lambda = 0.5$ value, the clump with radius 5 and 35 pc remains undestroyed even when $m_\phi = 10^{-21}$ eV, for all three different orbital cases: circular orbit with a galactocentric distance of 0.2 and 0.4 kpc, and eccentric orbit with $e = 0.6$. Only the extended $r_p = 80$ pc case gets destroyed ($\Pi_{80} \approx 1.4$ and 0.5 Gyr) when the stellar clump orbits at a galactocentric distance of 0.4 kpc for $m_\phi = 8 \times 10^{-22}$ eV and $m_\phi = 10^{-21}$ eV, respectively. For the other cases (circular orbit at a galctocentric distance of 0.2 kpc and eccentric orbit), even if the stellar clump is so extended, it remains undestroyed for 10 Gyr. Only when we increase the mass of the boson to $m_\phi = 2 \times 10^{-21}$ eV, the stellar clump gets destroyed for all r_p, and all orbital cases. This happens because the SFDM core radius is too small to guarantee its survival (~ 0.1 kpc).

When $\Lambda = 1$, the stellar clump only gets destroyed when the mass of the boson has reached the high value of $m_\phi = 2 \times 10^{-21}$ eV, which corresponds to a DM core radius of ~ 0.2 kpc). The clumps are destroyed earlier, when orbiting at a galactocentric distance of 0.4 kpc. For the orbit with a galactocentric distance of 0.2 kpc, the stellar clump only gets destroyed for the extended stellar clump with $r_p = 80$ pc. Lastly, when the clump is orbiting the eccentric orbit, the $r_p = 35$ and 80 pc clumps get destroyed within the first Gyr (0.61 and 0.46 Gyr respectively, see Table 1). Because the $r_p = 5$ pc clump is very compact, it overcomes the tidal effect of the SFDM halo, and gets destroyed later at ~ 3.77 Gyr.

When $\Lambda = 2$, we observe that the clump never gets destroyed, for any radius r_p case, or any orbital case. In Figure 5, we show the case of the stellar clump embedded in a SFDM halo with $m_\phi = 10^{-21}$ eV. For such a mass of the boson, and self-interacting parameter,

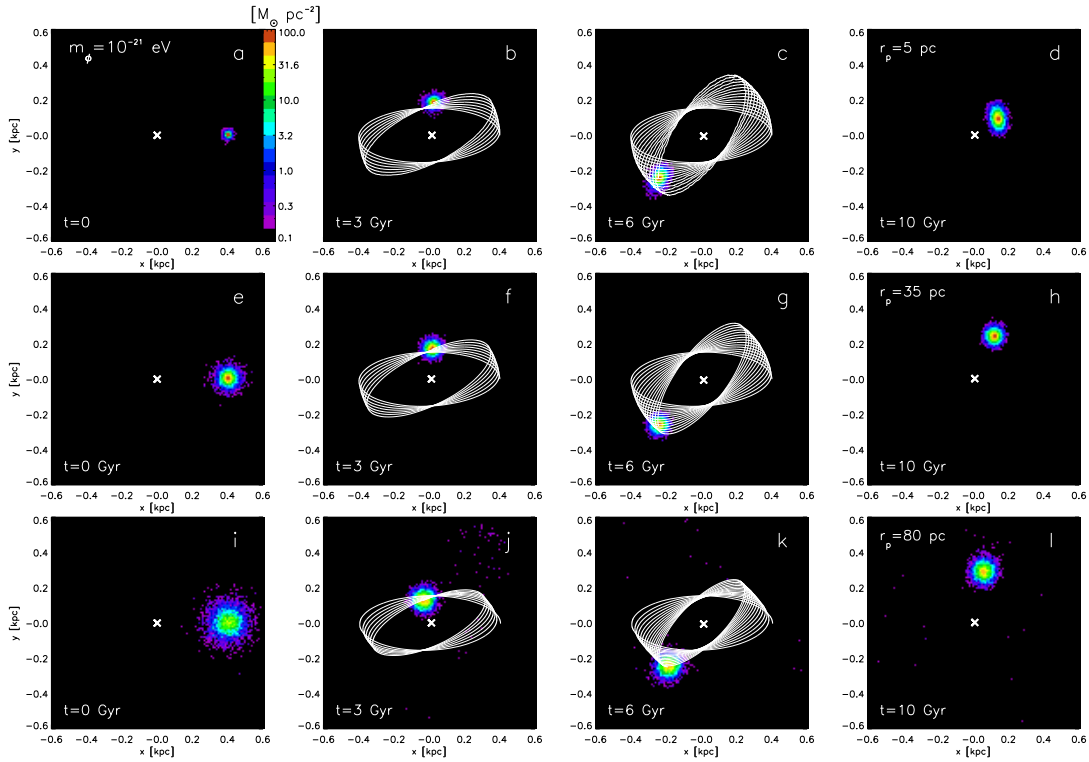

Figure 5. Time evolution (t = 0, 3, 6 and 10 Gyr) of the stellar clump's surface mass density in the Sextans dSph for a $m_\phi = 10^{-21}$ eV, and with a self interacting parameter of $\Lambda = 2$. In the top panels (*a*-*d*) we show the evolution of the compact $r_c = 5$ pc clump. In the middle panels (*e*-*h*) we show the time evolution of model with $r_c = 35$ pc. In the bottom panels (*i*-*l*) we show the time evolution for the extended model with a radius $r_c = 80$ pc. The white line shows the clump orbit in the (x, y)-plane (with apocenter at 0.4 kpc and pericenter at 0.1 kpc), and the white cross marks the centre of Sextans.

the SFDM core radius is 0.7 kpc, guaranteeing the survival of the clump. But it has to be noted, that in order to have a total mass of the DM halo $\gtrsim 10^8$ $M_\odot$, as suggested by [52], a $m_\phi \approx 10^{-22}$ eV is needed for a self interacting parameter $\Lambda = 2$.

For the same value of m_ϕ, the masses and core radii of the DM halos increase when Λ increases (see Table 1). For example, for a boson mass of 10^{-21} eV, the SFDM core radius is 0.35, 0.47 and 0.71 for $\Lambda = 0.5$, 1 and 2, respectively. Then, the permitted window for the mass m_ϕ of the bosonic particles is shifted to larger values ($m_\phi \approx 10^{-21}$ eV). We observe from our results, that the clump must be embedded in a SFDM halo with a mass $M \approx 10^7$ $M_\odot$, a "size" of the DM halo of $r_{95} \approx 0.8$ kpc, and a core radius of ≈ 0.4 kpc, in order to guarantee the survival of the stellar substructures.

5 Conclusions

In this work we consider an alternative to the CDM model, where ultra-light bosons are the main components of the DM halos. We constrain the mass of the ultra-light bosons (the SFDM particle) using as a tool the stellar substructures found in the Sextans dwarf galaxy. Using N-body simulations, we found that the survival of the stellar substructures is only possible if $m_\phi < 8 \times 10^{-22}$ eV for a self-interacting parameter $\Lambda = 0$. By imposing a realistic upper limit on the dynamical mass of Sextans, we place a lower limit of 1.2×10^{-23} eV.

Therefore, we have a possible mass window for the SF boson of 1.2×10^{-23} eVm_ϕ¡8×10^{-22} eV. These constraints imply SFDM halos with masses between $10^7 - 10^9$ $M_\odot$, maximum circular velocities between $48 - 8$ km s^{-1}, and sizes between $\sim 1 - 10$ kpc.

For the SFDM halos, where we include the self-interacting parameter, the upper limit grows with Λ. For example, for $\Lambda = 2$, the halos made up by bosons with a mass as high as $m_\phi = 2 \times 10^{-21}$ eV, accounts for the observed internal Sextans dynamics ($v_c \approx 8$ km s^{-1}), but the corresponding DM halo mass (1.3×10^7 M$_\odot$) would be to low for Sextans dwarf.

The preferred range for the mass of the boson, found in this work, derived from the dynamics of Sextans, is compatible with those given by other authors to ameliorate the problem of over-abundance of dark substructure [19, 62]. It is also in agreement with the mass range for the boson mass based on the dynamics of the UMi and the Fornax dSph galaxies [32].

The BEC/SFDM model has several challenges to overcome mainly at galactic scales and related to the baryonic dynamics. For example, [63] found discrepancies of one order of magnitude in the size of TFL BEC/SFDM halos estimated from dwarf galaxy dynamics and those derived from other galactic systems (strong lensing, rotation curves). Nevertheless, Robles & Matos [64] can reconcile the discrepancy when the finite temperature corrections in BEC/SFDM halos are considered [65]. The BEC/SFDM configurations in the TFL for ultra-light bosons are numerically unstable. However, the problem could be solved if the BEC/SFDM halos have angular momentum [66] or if the boson mass and the scattering length have an appropriate value [46]. The BEC/SFDM is a viable model to explain the nature of the DM, at cosmological and galactic scales, and therefore should be tested in more astrophysical systems.

Acknowledgments

We would like to thank Andreas Just, for his useful comments and suggestions. V.L. gratefully acknowledges support from the FRONTIER grant, and HB-L. J.M. acknowledges support from ESO Comité-Mixto 2010, and Gemini Fondecyt 32130024.

References

[1] A. Klypin, A. V. Kravtsov, O. Valenzuela, and F. Prada, *Where Are the Missing Galactic Satellites?*, Astrophys. J. 522 (1999) 82, [arXiv:astro-ph/9901240].

[2] P.J.E. Peebles and A. Nusser, *Nearby galaxies as pointers to a better theory of cosmic evolution*, Nature 465 (2010) 565, [arXiv:1001.1484].

[3] F. C. van den Bosch, B. E. Robertson, J. J. Dalcanton and W. J. G. de Blok, *Constraints on the Structure of Dark Matter Halos from the Rotation Curves of Low Surface Brightness Galaxies*, Astron. J. 119 (2000) 1579, [arXiv:astro-ph/9911372].

[4] J. T. Kleyna, M. I. Wilkinson, G. Gilmore and N. W. Evans, *A Dynamical Fossil in the Ursa Minor Dwarf Spheroidal Galaxy*, Astrophys. J. 588L (2003) 21, [*Erratum: ibid* 589L (2003) 59], [arXiv:astro-ph/0304093].

[5] W. J. G. de Blok and A. Bosma, *High-resolution rotation curves of low surface brightness galaxies*, Astron. Astrophys. , 385 (2002) 816, [arXiv:astro-ph/0201276].

[6] S. J. Sin, *Late-time phase transition and the galactic halo as a Bose liquid*, Phys. Rev. D. 50 (1994) 3650, [arXiv:hep-ph/9205208].

[7] S. U. Ji and S. J. Sin, *Late-time phase transition and the galactic halo as a Bose liquid. II. The effect of visible matter*, Phys. Rev. D. 50 (1994) 3655, [arXiv:hep-ph/9409267]

[8] J.-W. Lee and I.-G. Koh, *Galactic halos as boson stars*, Phys. Rev. D. 53 (1996) 2236, [arXiv:hep-ph/9507385].

[9] P. J. E. Peebles, *Noninteracting dark matter*, Phys. Rev. D. 60 (1999) 103506, [arXiv:astro-ph/9904396].

[10] T. Matos, F. S. Guzmán F. S. and L. A. Ureña-Lopez, *Scalar field as dark matter in the universe* Class. Quant. Grav. 17 (2000) 1707, [arXiv:astro-ph/9908152].

[11] F. S. Guzmán and T. Matos, *LETTER TO THE EDITOR: Scalar fields as dark matter in spiral galaxies*, Class. Quant. Grav. 17 (2000) L9, [arXiv:gr-qc/9810028].

[12] J. Magaña and T. Matos, *A brief Review of the Scalar Field Dark Matter model*, J. Phys. Conf. S. 378 (2012) 012012, [arXiv:1201.6107].

[13] A. Suárez, V. Robles and T. Matos, *A Review on the Scalar Field/ Bose-Einstein Condensate Dark Matter Model*, Astrophys. Space Science Proc. 38 (2014) 107, [arXiv:1302.0903].

[14] T. Matos and A. Suárez, *Finite temperature and dissipative corrections to the Gross-Pitaevskii equation from $\lambda\Phi^4$ one-loop contributions*, 2011, Europhys. Lett., 96 (2011) 56005, [arXiv:1110.3114].

[15] T. Matos and E. Castellanos, *Bose gas to Bose-Einstein Condensate by the Phase Transition of the Klein-Gordon equation*, 2012, [arXiv:1207.4416].

[16] E. Castellanos and T. Matos, *Critical Temperature Associated to Symmetry Breaking of Klein–Gordon fields versus Condensation Temperature in a Weakly interacting Bose–Einstein Gas*, 2012, [arXiv:1202.3793].

[17] E. Castellanos, A. Macías and D. Núñez, *Scalar Field as a Bose-Einstein Condensate?*, 2013, [arXiv:1310.3319].

[18] M. S. Turner, *Coherent scalar-field oscillations in an expanding universe*, Phys. Rev. D. 28 (1983) 1243.

[19] T. Matos and L. A. Ureña-Lopez, *Further analysis of a cosmological model with quintessence and scalar dark matter*, Phys. Rev. D. 63 (2001) 063506, [arXiv:astro-ph/0006024].

[20] T. Matos, A. Vázquez-González and J. Magaña, *ϕ^2 as dark matter*, Mon. Non. Roy. Astron.

Soc. 393 (2009) 1359, [arXiv:0806.0683].

[21] A. Suárez and T. Matos, *Structure formation with scalar-field dark matter: the fluid approach*, Mon. Non. Roy. Astron. Soc. 416 (2011) 87, [arXiv:1101.4039].

[22] J. Magaña, A. Suárez, T. Matos and F. J. Sánchez-Salcedo, *Structure formation with scalar field dark matter: the field approach*, J. Cosmol. Astropart. Phys. JCAP10 (2012) 003, [arXiv:1204.5255].

[23] T. Harko, *Evolution of cosmological perturbations in Bose-Einstein condensate dark matter*, Mon. Non. Roy. Astron. Soc. 413 (2011) 3095, [arXiv:1101.3655].

[24] T. Harko, *Bose-Einstein condensation of dark matter solves the core/cusp problem*, J. Cosmol. Astropart. Phys. JCAP05 (2011) 022, [arXiv:1105.2996].

[25] T. Harko, *Cosmological dynamics of dark matter Bose-Einstein condensation*, Phys. Rev. D. 83 (2011) 123515, [arXiv:1105.5189].

[26] P. H. Chavanis, *Mass-radius relation of Newtonian self-gravitating Bose-Einstein condensates with short-range interactions. I. Analytical results*, Phys. Rev. D. 84 (2011) 043531, [arXiv:1103.2050].

[27] P. H. Chavanis, *Mass-radius relation of Newtonian self-gravitating Bose-Einstein condensates with short-range interactions. II. Numerical results*, Phys. Rev. D. 84 (2011) 043532, [arXiv:1103.2054].

[28] P. H. Chavanis, *Growth of perturbations in an expanding universe with Bose-Einstein condensate dark matter*, Astron. Astrophys. 537 (2012) A127, [arXiv:1103.2698].

[29] I. Rodríguez-Montoya, J. Magaña, T. Matos and A. Pérez-Lorenzana, *Ultra Light Bosonic Dark Matter and Cosmic Microwave Background*, Astrophys. J. 72 (2010) 1509, [arXiv:0908.0054].

[30] T. Rindler-Daller and P. R. Shapiro, *Angular momentum and vortex formation in Bose-Einstein-condensed cold dark matter haloes*, Mon. Non. Roy. Astron. Soc. 422 (2012) 135, [arXiv:1106.1256].

[31] B. Li, T. Rindler-Daller and P. R. Shapiro, *Cosmological constraints on Bose-Einstein-condensed scalar field dark matter*, Phys. Rev. D. 89 (2013) 083536, [arXiv:1310.6061].

[32] V. Lora, J. Magaña, A. Bernal, F. J. Sánchez-Salcedo and E. K. Grebel, *On the mass of ultra-light bosonic dark matter from galactic dynamics*, J. Cosmol. Astropart. Phys. JCAP02 (2012) 011, [arXiv:1110.2684].

[33] V. H. Robles and T. Matos, *Flat central density profile and constant dark matter surface density in galaxies from scalar field dark matter*, Mon. Non. Roy. Astron. Soc. 422 (2012) 282, [arXiv:1201.3032)].

[34] J. F. Navarro, C. S. Frenk and S. D. M. White, *The Structure of Cold Dark Matter Halos*, Astrophys. J. 462 (1996) 563, [arXiv:astro-ph/9508025].

[35] J. T. Kleyna, M. I. Wilkinson, N. W. Evans and G. Gilmore, *A photometrically and kinematically distinct core in the Sextans dwarf spheroidal galaxy*, Mon. Non. Roy. Astron. Soc. 354 (2004) L66, [arXiv:astro-ph/0409066].

[36] M. G. Walker, M. Mateo, E. W. Olszewski, J. K. Pal, B. Sen and M. Woodroofe, *On Kinematic Substructure in the Sextans Dwarf Spheroidal Galaxy*, Astrophys. J. 642 (2006) L41, [arXiv:astro-ph/0603694].

[37] G. Battaglia, E. Tolstoy, A. Helmi, M. Irwin, P. Parisi, V. Hill and P. Jablonka, *Study of the Sextans dwarf spheroidal galaxy from the DART Ca II triplet survey*, Mon. Non. Roy. Astron. Soc. 411 (2011) 1013, [arXiv:1009.4857].

[38] R. Ruffini and S. Bonazzola, *Systems of Self-Gravitating Particles in General Relativity and the*

Concept of an Equation of State, Phys. Rev. 187 (1969) 1767.

[39] Seidel, E. & Suen, W.-M., *Oscillating soliton stars*, Phys. Rev. Lett. 66 (1991) 1659.

[40] Chi-Wai Lai PhD Thesis.
http://laplace.phas.ubc.ca/Members/matt/Doc/Theses/
Phd/lai.pdf

[41] A. Bernal PhD Thesis.
http://www.fis.cinvestav.mx/thesis/index.php/thesis

[42] R. Friedberg, T. D. Lee and Y. Pang, *Mini-soliton stars*, Phys. Rev. D. 35 (1987) 3640.

[43] F. S. Guzmán and L. A. Ureña-López, *Evolution of the Schrödinger-Newton system for a self-gravitating scalar field*, Phys. Rev. D. 69 (2004) 124033, [arXiv:gr-qc/0404014].

[44] F. S. Guzmán, F. D. Lora-Clavijo, J. J. González-Avilés and F. J. Rivera-Paleo, *Stability of BEC galactic dark matter halos* J. Cosmol. Astropart. Phys. JCAP09 (2013) 034, [arXiv:1308.4925].

[45] V. T. Toth, *Self-gravitating Bose-Einstein condensates and the Thomas-Fermi approximation*, 2014, [arXiv:1402.0600].

[46] J. C. C. de Souza and M. O. C. Pires, *Discussion on the energy content of the galactic dark matter Bose-Einstein condensate halo in the Thomas-Fermi approximation*, J. Cosmol. Astropart. Phys. JCAP03 (2014) 010, [arXiv:1401.6142].

[47] M. L. Mateo, *Dwarf Galaxies of the Local Group* Ann. Rev. Astron. Astrophys. 36 (1998) 435 [arXiv:astro-ph/9810070].

[48] E. L. Łokas, *The mass and velocity anisotropy of the Carina, Fornax, Sculptor and Sextans dwarf spheroidal galaxies*, Mon. Non. Roy. Astron. Soc. 394 (2009) L102, [arXiv:0901.0715].

[49] M. Irwin and D. Hatzdimitriou, *Structural parameters for the Galactic dwarf spheroidals*, Mon. Non. Roy. Astron. Soc. 277 (1995) 1354.

[50] T. Karlsson, J. Bland-Hawthorn, K. C. Freeman, and J. Silk, *The Chemical Signature of a Relic Star Cluster in the Sextans Dwarf Spheroidal Galaxy –Implications for Near-field Cosmology*, Astrophys. J. 759 (2012) 111, [arXiv:1201.5376].

[51] M. G. Walker, M. Mateo, E. W. Olszewski, O. Y. Gnedin, X. Wang, B. Sen and M. Woodroofe, *Velocity Dispersion Profiles of Seven Dwarf Spheroidal Galaxies* Astrophys. J. 667 (2007) L53, [arXiv:0708.0010].

[52] L. E. Strigari, J. S. Bullock, M. Kaplinghat, J. Diemand, K. Kuhlen and P. Madau, *Redefining the Missing Satellites Problem* Astrophys. J. 669 (2007) 676, [arXiv:0704.1817]

[53] L. E. Strigari, J. S. Bullock, M. Kaplinghat, J. D. Simon, M. Geha, B. Willman and M. G. Walker, *A common mass scale for satellite galaxies of the Milky Way* Nat. 454 (2008) 1096, [arXiv:0808.3772].

[54] C. A. Vera-Ciro, L. V. Sales, A. Helmi and J. F. Navarro, *The shape of dark matter subhaloes in the Aquarius simulations*, Mon. Non. Roy. Astron. Soc. 439 (2014) 2863, [arXiv:1402.0903].

[55] H. C. Plummer, *On the problem of distribution in globular star clusters*, Mon. Non. Roy. Astron. Soc. 71 (1911) 460.

[56] J. Binney and S. Tremaine, Galactic Dynamics, 2nd edn. Princeton Univ. Press, Princeton, NJ, 2008.

[57] M. Fellhauer, P. Kroupa, H. Baumgardt, R. Bien, C. M. Boily, R. Spurzem and N. Wassmer, *SUPERBOX - an efficient code for collisionless galactic dynamics*, New Astron. 5 (2000) 305, [arXiv:astro-ph/0007226]

[58] R. Bien, T. Brandt and A. Just, *Simulating sinking satellites with superbox-10*, Mon. Non. Roy.

Astron. Soc. 428 (2013) 1631, [arXiv:1210.1736].

[59] A. R. Zentner and J. S. Bullock, *Halo Substructure and the Power Spectrum*, Astrophys. J. 598 (2003) 49, [arXiv:astro-ph/0304292].

[60] J. Peñarrubia, A. W. McConnachie and J. F. Navarro, *The Cold Dark Matter Halos of Local Group Dwarf Spheroidals*, Astrophys. J. 672 (2008) 904, [Erratum ibid 687 (2008) 1460], [arXiv:astro-ph/0701780].

[61] M. L. M. Collins, S. C. Chapman, R. M. Rich et. al, *The Masses of Local Group Dwarf Spheroidal Galaxies: The Death of the Universal Mass Profile*, Astrophys. J. 783 (2014) 7, [arXiv:1309.3053].

[62] W. Hu, R. Barkana and A. Gruzinov A., *Fuzzy Cold Dark Matter: The Wave Properties of Ultralight Particles*, Phys. Rev. Lett. 85 (2000) 1158, [arXiv:astro-ph/0003365].

[63] A. X. González-Morales, A. Diez-Tejedor, L. A. Ureña-Lṕez and O. Valenzuela, *Hints on halo evolution in scalar field dark matter models with galaxy observations*, Phys. Rev. D. 87 (2013) 021301, [arXiv:1211.6431].

[64] V. H. Robles and T. Matos, *Strong lensing with finite temperature scalar field dark matter*, Phys. Rev. D. 88 (2013) 083008, [arXiv:1302.5944].

[65] V. H. Robles and T. Matos, *Exact Solution to Finite Temperature SFDM: Natural Cores without Feedback*, Astrophys. J. 763 (2013) 19, [arXiv:1207.5858].

[66] F. S. Guzmán, F. D. Lora-Clavijo, J. J. González-Avilés and F. J. Rivera-Paleo, *Rotation curves of rotating Galactic Bose-Einstein condensate dark matter halos*, Phys. Rev. D. 89 (2014) 063507 [arXiv:1310.3909].

Table 1. Destruction times (Π) of the stellar clump in Sextans for the $\Lambda = 0$, 0.5, 1 and 2 case, for different values of m_ϕ. The sub-index in Π corresponds to the plummer radius of the clump (5, 35 and 80 pc). The SF boson mass, ϵ, the total mass M; the radius at which 95% of the total mass is contained, r_{95}; and the core radius, r_{core}; are also given for each of the models.

Λ	m_ϕ ($10^{-22} eV$)	ϵ (10^{-5})	M (10^8 $M_\odot$)	r_{95} (kpc)	r_{core} (kpc)	Π_5 (Gyr)	Π_{35} (Gyr)	Π_{80} (Gyr)	Orbit type
0	0.1	22.7996	62.8	10.6555	5.4345	>10	>10	>10	circular, x=200 pc
0	0.1	22.7996	62.8	10.6555	5.4345	>10	>10	>10	circular, x=400 pc
0	1.0	7.3881	2.035	3.2882	1.6770	>10	>10	>10	circular, x=200 pc
0	1.0	7.3881	2.035	3.2882	1.6770	>10	>10	>10	circular, x=400 pc
0	5.0	3.8120	0.21	1.2746	0.6501	>10	>10	>10	circular, x=200 pc
0	5.0	3.8120	0.21	1.2746	0.6501	>10	>10	~ 6	circular, x=400 pc
0	7.0	3.5477	0.139	0.9782	0.4989	>10	>10	>10	circular, x=200 pc
0	7.0	3.5477	0.139	0.9782	0.4989	>10	>10	~ 0.5	circular, x=400 pc
0	8.0	3.5152	0.121	0.8638	0.4406	>10	>10	>10	circular, x=200 pc
0	8.0	3.5152	0.121	0.8638	0.4406	>10	~ 1.7	~ 0.35	circular, x=400 pc
0	8.0	3.5152	0.121	0.8638	0.4406	>10	~ 4.53	~ 0.87	excentric, e=0.6
0	9.0	3.5452	0.108	0.7614	0.3883	>10	>10	>10	circular, x=200 pc
0	9.0	3.5452	0.108	0.7614	0.3883	~ 7.72	~ 0.65	~ 0.2	circular, x=400 pc
0	9.0	3.5452	0.108	0.7614	0.3883	~ 8.08	~ 1.32	~ 0.74	excentric, e=0.6
0	10	3.6305	0.1	0.6691	0.3412	>10	>10	~ 3	circular, x=200 pc
0	10	3.6305	0.1	0.6691	0.3412	~ 5.3	~ 0.4	~ 0.15	circular, x=400 pc
0	10	3.6305	0.1	0.6691	0.3412	~ 6	~ 0.97	~ 0.58	excentric, e=0.6
0.5	0.1	22.7423	95.79	11.2252	4.5685	>10	>10	>10	circular, x=200 pc
0.5	0.1	22.7423	95.79	11.2252	4.5685	>10	>10	>10	circular, x=400 pc
0.5	1.0	7.3124	3.08	3.4911	1.4208	>10	>10	>10	circular, x=200 pc
0.5	1.0	7.3124	3.08	3.4911	1.4208	>10	>10	>10	circular, x=400 pc
0.5	5.0	3.5684	0.3006	1.4308	0.5823	>10	>10	>10	circular, x=200 pc
0.5	5.0	3.5684	0.3006	1.4308	0.5823	>10	>10	>10	circular, x=400 pc
0.5	7.0	3.1875	0.1918	1.1441	0.4656	>10	>10	>10	circular, x=200 pc
0.5	7.0	3.1875	0.1918	1.1441	0.4656	>10	>10	>10	circular, x=400 pc
0.5	8.0	3.0788	0.1621	1.0364	0.4218	>10	>10	>10	circular, x=200 pc
0.5	8.0	3.0788	0.1621	1.0364	0.4218	>10	>10	~ 1.4	circular, x=400 pc
0.5	8.0	3.0788	0.1621	1.0364	0.4218	>10	>10	>10	excentric, e=0.6
0.5	10	2.9701	0.1251	0.8595	0.3498	>10	>10	>10	circular, x=200 pc
0.5	10	2.9701	0.1251	0.8595	0.3498	>10	>10	~ 0.5	circular, x=400 pc
0.5	10	2.9701	0.1251	0.8595	0.3498	>10	>10	~ 1.38	excentric, e=0.6
0.5	20	4.2782	0.0901	0.2983	0.1214	~ 1.75	~ 0.25	~ 0.13	circular, x=200 pc
0.5	20	4.2782	0.0901	0.2983	0.1214	~ 2.2	~ 0.12	~ 0.05	circular, x=400 pc
0.5	20	4.2782	0.0901	0.2983	0.1214	~ 1.6	~ 0.3	~ 0.27	excentric, e=0.6
1	1.0	7.2623	4.693	3.7225	1.7387	>10	>10	>10	circular, x=200 pc
1	1.0	7.2623	4.693	3.7225	1.7387	>10	>10	>10	circular, x=400 pc
1	10	2.6492	0.1712	1.0204	0.4766	>10	>10	>10	circular, x=200 pc
1	10	2.6492	0.1712	1.0204	0.4766	>10	>10	>10	circular, x=400 pc
1	10	2.6492	0.1712	1.0204	0.4766	>10	>10	>10	excentric, e=0.6
1	20	2.8164	0.091	0.4799	0.2241	>10	>10	~ 1.5	circular, x=200 pc
1	20	2.8164	0.091	0.4799	0.2241	~ 3.43	~ 0.1	~ 0.09	circular, x=400 pc
1	20	2.8164	0.091	0.4799	0.2241	~ 3.77	~ 0.61	~ 0.46	excentric, e=0.6
2	1.0	7.2202	0.9723	4.2634	2.3910	>10	>10	>10	circular, x=200 pc
2	1.0	7.2202	0.9723	4.2634	2.3910	>10	>10	>10	circular, x=400 pc
2	10	2.4260	0.3267	1.2688	0.7116	>10	>10	>10	circular, x=200 pc
2	10	2.4260	0.3267	1.2688	0.7116	>10	>10	>10	circular, x=400 pc
2	10	2.4260	0.3267	1.2688	0.7116	> 10	> 10	> 10	excentric, e=0.6
2	20	1.9124	0.1288	0.8048	0.4513	>10	>10	>10	circular, x=200 pc
2	20	1.9124	0.1288	0.8048	0.4513	>10	>10	>10	circular, x=400 pc
2	20	1.9124	0.1288	0.8048	0.4513	>10	>10	>10	excentric, e=0.6